Flow Dynamics Between Two Car Models: Influence Of The Intervehicle Distance

Oumaima Oussairan, Béatrice Patte-Rouland, Franck Lefebvre, Carole Gobin, G. Godard, Frédéric Murzyn, Emilien Varea, Georges Fokoua, Florian Lespinasse

Flow Dynamics Between Two Car Models: Influence Of The Intervehicle Distance

Oumaima Oussairan, Béatrice Patte-Rouland, Franck Lefebvre, Carole Gobin, G. Godard, Frédéric Murzyn, Emilien Varea, Georges Fokoua, Florian Lespinasse

Flow Dynamics Between Two Car Models: Influence Of The Inter-vehicle Distance

O. Oussairan[1,2,*], F. Lefebvre[1], C. Gobin[1], G. Godard[1], F. Lespinasse[1], G. Fokoua[3], E. Varéa [1], B. Patte-Rouland[1] and F. Murzyn[2]

1: Dept. of Turbulence, Atomisation, Sprays et Chaos, CORIA Lab, The University of Rouen, France
2: Dept. of Mechanical Engineering, Air Quality and Depollution Group, ESTACA West Campus, France
3: Dept. of Mechanical Engineering, Air Quality and Depollution Group, 2 ESTACA Paris Saclay Campus, France
*Corresponding author: oumaima.oussairan@estaca.fr

Keywords: SPIV, 2D LDV, Flow dynamics, Ahmed body, Influence of inter-vehicle distance.

ABSTRACT

Air pollution is a crucial issue since it is one of the major causes for worldwide deaths. Car drivers and passengers are daily exposed to high level of pollutant concentrations. The particles emitted from the tailpipe can disperse in the wake of the vehicle and then infiltrate the following car cabin. It has been demonstrated that the dynamics of such particles are highly affected by the properties of the flow downstream the emitting vehicle (Rodriguez et al., 2020). In the present paper, the flow characterization in the wake of a simplified car model followed by a second vehicle is performed. Reduced-scaled Ahmed bodies are used. The upstream velocity is set to $U_\infty = 14.3\,\mathrm{m\,s^{-1}}$, corresponding to a Reynolds number based on the simplified model's height ($h_c = 54\,\mathrm{mm}$) of Re = 49500. Two leading vehicles with two different rear slant angles ($\varphi = 0°$, $25°$) are considered. Two sets of experiments are carried out, one in the wind tunnel at ESTACA and the other in the wind tunnel at CORIA'lab. In the first measurement campaign, 2D LDV is used and six inter-vehicle distances ranging from d = 0.93 h_c to 5.56 h_c are considered and presented. The ITTT (Interarrival Time and Transit Time) method developed by Rodriguez et al. (2018) is applied to LDV data in order to ensure reliable results. Mean and turbulent properties of the wake between the two vehicles are described. The role of the rear slant angle is highlighted. A critical distance above which the followed vehicle has an insignificant influence on the flow topology downstream of the leading vehicle is identified. For further details, and taking into consideration the first results (from LDV measurements), Stereo-PIV measurements are used to get access to the three components of the velocity. Due to time constraint, only three inter-vehicle distances are discussed in this paper (0.93 h_c, 1.85 h_c and 3.70 h_c). The SPIV results validate those obtained from LDV measurements and provide complementary information. The sensitivities of the bi-stability of the transverse velocity to the short inter-vehicle distance (0.93 h_c) and to the slant rear angle are investigated. SPIV measurements are then correlated with LDA measurements taking into account this behavior. These measurements are completed by further measurements of concentrations of the exhausted particles from the tailpipe. They will be discussed in another paper.

1. Introduction

Vehicles, heating systems for houses, burning of waste and industries are among the main sources of pollutants, which can be gases and particles. According to a recent environmental research from Harvard University, fossil fuel related air pollution is responsible for 20% of deaths (Torjesen, 2021). Ground vehicles emit particles, including Ultrafine Particles (UFP), which have two major origins. On the one hand, there are non-exhaust related particles emitted from the brakes, resuspension and tyre/road wear. On the other hand, exhaust related particles are emitted from the tailpipe. All these particles affect the surrounding environment and are harmful for people. Drivers and commuters can be exposed to high levels of pollutant concentrations, above the standards defined by local health authorities, as the car cabin is a micro-environment where pollutants can accumulate. It has been demonstrated that they can enter the passenger compartment through leakages and ventilation system. To date, little attention has been focused on the influence of the interaction between two vehicles on the concentration fields of the pollutants emitted in the wake of a leading vehicle (LV). However, understanding influence of the following vehicle (FV) on the wake properties of the LV is essential to examine the dispersion of the UFP in its wake. It is obvious that the flow downstream the LV is affected by the inter-vehicle distance. Essel et al. (2020) performed experimental PIV measurements between two in-line Ahmed bodies for single inter-vehicle distance d (d $= 0.75L_c$, $L_c = 196\,\mathrm{mm}$ being the length of the model). This distance is equivalent to d = 1.85 h_c in our case. In the presence of the FV, they found that the recirculation region behind the square back Ahmed body increases while the one behind the slant rear-end bodies decreases.

In the works of Grandemange et al. (2013), the flow around a 1:4 scale model square back Ahmed body at Re = 920,000 was investigated. They found that a large recirculation region is dominant part in the wake. They well documented the bi-stability behavior resulting from a dynamic switch between two symmetric configurations with respect to the vertical center plane. This explains that the symmetric flow topology arise from averaging two asymmetric configurations. Herry et al. (2011) also found that the flow developping downstream double backward facing step presents a bi-stable behavior for different upstream conditions (Re ranging from 5,000 to 80,000, based on the first step height).

The present work aims first at studying and discussing the influences of a FV and of the rear slant angle on the wake flow topology of the LV for six different inter-vehicle distances. A second interest is reported for the bi-stability behavior seen in the third component of the velocity vector. LDV and SPIV measurements are performed. The simplified car models named Ahmed bodies were chosen. The paper is organized as follows. In section 2, the instruments and experimental set- ups are described. Section 3 is devoted to results: both mean and turbulent flow properties are considered. Then, conclusions and perspectives are presented in section 4. A new developpement presented in this paper deals with the time resolved flow dynamics in order to understand how the flow structures may be capable to entrap and/or disperse exhaust particles.

2. Instrumentation and measurement techniques

2.1. Geometry

Simplified car models known as Ahmed body (Ahmed et al., 1984) are used in the experiments. They are well-known in aerodynamic studies (Leclerc, 2008; Thacker et al., 2012) regarding their ability to reproduce similar physical structures that develop in the wake of road vehicles. Ahmed et al. (1984), Spohn & Gilliéron (2002), and Lienhart & Becker (2003) presented a detailed description of the flow structures downstream Ahmed bodies. These strucures and the associated drag force are highly dependent of the rear slant angle of the car. Three classes may be distinguished:

- $\varphi <\sim 10°$: the flow is fully attached on the rear angle and two counter rotating vortices are developed in the close wake. In addition, a toric shape is observed in the recirculation region;
- $\sim 10° < \varphi <\sim 30°$: the flow pattern is partially separated from the rear slant angle. Longitudinal vortices appear, which take birth from the lateral sides of the vehicle. The toric shape is still observed.
- $\varphi >\sim 30°$: the behavior of the flow is similar to that observed for $\varphi <\sim 10°$. However, the flow is fully detached on the rear slant and the longitudinal votices do not longer exist.

The experiments are performed with a 0.19 scaled Ahmed body with two rear slant angles $\varphi = 0°$ and $\varphi = 25°$. The car models are $0.196\,\mathrm{m}$ in length (L_c), $0.054\,\mathrm{m}$ in height (h_c) and $0.073\,\mathrm{m}$ in width (l_c). They are fixed on the floor of the test section using a cylindrical rod ($5\,\mathrm{mm}$ diameter). Four cylindrical stilts are used ($15\,\mathrm{mm}$ and $6\,\mathrm{mm}$ in height and diameter respectively). Figure 1 presents a sketch of the simplified car considered for the measurements. The model is set at the centerline of the test section at 3.4 h_c from its entrance. The coordinate system o(x, y, z) is shown in the Fig. 1, x in the streamwise direction, y in vertical direction (normal to the ground) and z in the transverse direction. It has its origin at the bottom of the rear face at the centerline of the test section. The coordinate system is also presented as (x^*, y^*, z^*), which represents the dimensionless distances with respect to h_c. The dimensionless ground clearance was $\mathrm{H}_g = \mathrm{h}_g/\mathrm{h}_c = 0.28$. No correction accounting for wall effects was considered as the models were designed to keep a blockage coefficient below 5% (West & Apelt, 1982).

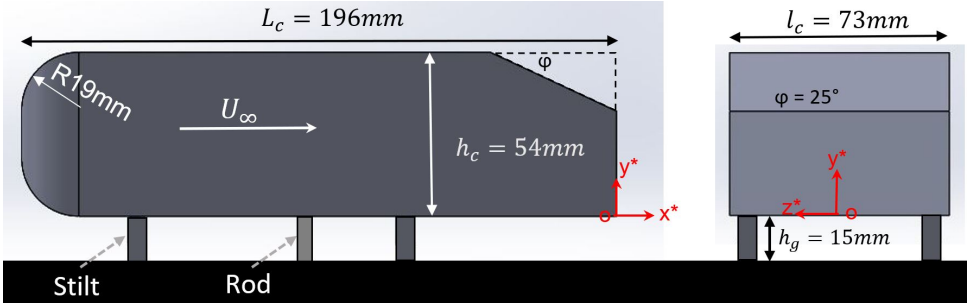

Figure 1. Sketches of the car model: side (left) and rear (right) views.

The incoming air flow velocity (U_∞) is determined to keep constant the ratio between the speed of the car and the velocity of the exhaust particles at the exit of the tailpipe (U_{tp}) in real-life conditions. As a consequence, the upstream velocity considered in the measurements is $\mathrm{U}_\infty = 14.3\,\mathrm{m\,s^{-1}}$. The velocity vector is defined as $\vec{u}$ = u$\vec{e_x}$ + v$\vec{e_y}$ + w$\vec{e_z}$.

2.2. 2D LASER Doppler Velocimetry (LDV) measurements

The experiments are conducted in the open circuit wind tunnel located at ESTACA West Campus (model EA 103). The maximum wind speed is $U_{max} = 40\,\mathrm{m\,s^{-1}}$. The test section is $1\,\mathrm{m}$ in length and $0.3\,\mathrm{m}$ in both height and width. The calibration of this facility with an empty test section was performed in a past work by Rodriguez (2018). Regarding the incoming flow, the relevant conclusions indicated that the turbulence intensity is below 1% on the streamwise direction, outer the boundary layer which thickness (δ) was about $12\,\mathrm{mm}$ at the exit of the test section.

The velocity measurements are recorded using a 2D LDV system manufactured by DANTEC Dynamics, model 2D Flow Explorer. Two pairs of LASER beams (wavelengths of $660\,\mathrm{nm}$ and $785\,\mathrm{nm}$, respectively) are emitted to record the horizontal and the vertical velocity components, respectively. The fringe spacings are $5.45\,\mu\mathrm{m}$ and $6.40\,\mathrm{nm}$ in the horizontal and vertical directions, respectively. The measuring volumes are of $0.17 \times 0.17 \times 2.8\,\mathrm{mm}^3$ and $0.20 \times 0.20 \times 3.34\,\mathrm{mm}^3$ for the horizontal and vertical velocity components, respectively. The focal length is $500\,\mathrm{mm}$ and Bragg cell frenquency shifting is $80\,\mathrm{MHz}$.

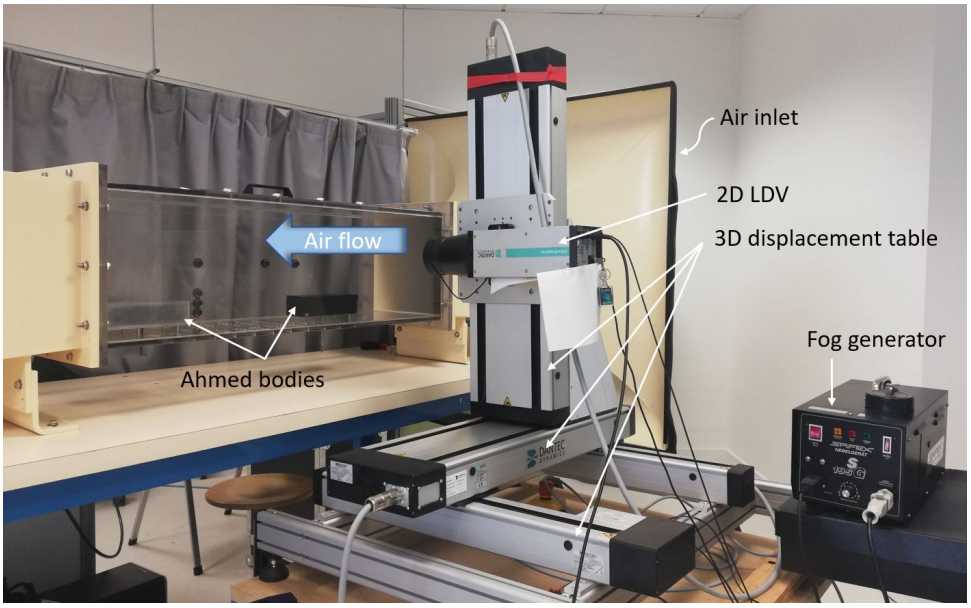

Figure 2. Experimental set-up for velocity measurements.

The 2D LDV system is mounted on a 3D displacement table. The range of displacement is $410 \times 410 \times 410\,\mathrm{mm}^3$ in the x, y and z directions. The control of the LDV and the displacement systems

is ensured through the BSA Flow Software (v5.03.00). Considering the recommandations of Algieri et al. (2005), the seeding particles generated for these measutements are made of a mixture of diethylene glycol $C_4H_{10}O_3$ and water (SAFEX Inside Nebelfluid Extra Clean provided by DANTEC). Particles are seeded by the SAFEX S 195 G fog generator. The mean diameter of the particles is $1.068\,\mu\mathrm{m}$. A picture of the experimental set-up is showed in the Fig. 2.

2.3. Stereo Particle Image Velocimetry (SPIV) measurements

SPIV measurements are carried out in the closed-circuit wind tunnel located at CORIA (University of Rouen, France). The maximun velocity is of $16\,\mathrm{m\,s^{-1}}$. The test section is $0.4\,\mathrm{m} \times 0.4\,\mathrm{m}$ with a length of $2.5\,\mathrm{m}$. The SPIV technique is used to obtain the three components of velocity. A ND-YAG LASER-Photonics DM150-532DH- cadenced at 20 kHz is used for flow illumination. A LASER sheet of $45\,\mathrm{mm} \times 70\,\mathrm{mm}$ is generated using a cylindrical lens (f = $-50\,\mathrm{mm}$) followed by a spherical lens (f = $500\,\mathrm{mm}$). The LASER sheet is placed perpendicularly between the 2 Ahmed bodies. Seeding is obtained using mixing of water and glycol. Size repartition of the particles is homogeneous (mean diameter of $25\,\mu\mathrm{m}$). Two cameras Phantom V2012 coupled with two Scheimpflug mounts and visible AF NIKKOR 80 – 220 f/2.8 are placed on either side of the LASER sheet with an angle of $32.4°$. Each camera records particle images, which are post-processed with 'DaVis 10.2.0' software, provided by La Vision. The cameras and the optical instuments are mounted on a 3D-displacement system. In order to have the same experimental conditions, the two Ahmed bodies are designed by 3D printing in the CORIA'Lab with a scale of 0.19, one of $\varphi = 0°$ and another of $\varphi = 25°$. The upstream velocity is set at $U_\infty = 14.3\,\mathrm{m\,s^{-1}}$. A picture of the experimental set-up is given in Fig.3.

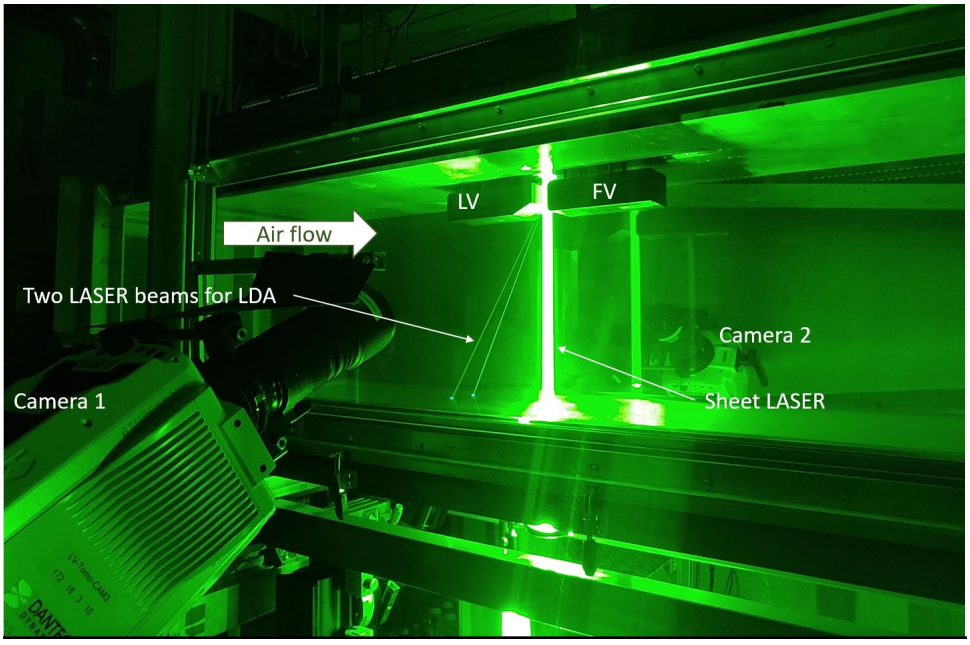

Figure 3. Experimental set-up for SPIV measurements.

In addtition to SPIV measurements, 1D LDA measurements are performed in specific points to get access to the third component of the velocity (w). The wavelength of LASER beams is $488\,\mathrm{nm}$ and the focal length is $500\,\mathrm{mm}$. The number of frange is 35 and the inter-fringe spacing is $3.252\,\mu\mathrm{m}$. The volume of measurement is such as: $0.1166 \times 0.1162 \times 1.549\,\mathrm{mm}^3$. The acquisition is carried out in Burst mode. It lasts $9\,\mathrm{s}$ with 5000 samples. The acquisition and the setting of the associated parameters are done on the BSA3 software of *Dantec*.

3. Data acquisition process and analysis

3.1. LDV data

Six inter-vehicle distances (d) are considered going from $50\,\mathrm{mm}$ to $300\,\mathrm{mm}$ with a step of $50\,\mathrm{mm}$. The corresponding dimensionless distances ($\mathrm{d}^* = \dfrac{d}{h_c}$) are 0.93, 1.85, 2.78, 3.70, 4.63 and 5.56. Data acquisition lasts $90\,\mathrm{s}$ at each point in order to ensure the convergence and the statistical accuracy of the data, and a maximum of 5000 samples were recorded. In this paper, we only present the measurements corresponding at the centerline of the test section ($\mathrm{z}^* = 0$). On the y-axis, measurements are performed according to the following meshing: from y^* = 0 to 1.02 with dimensionless step of $\mathrm{y}_s^* = \dfrac{y_s}{h_c} = 0.09$ (12 positions) on the y-axis and a supplementary upper point was fixed at y^* = 1.2 (1 position). The meshing in the longituinal direction depends on the inter-vehicle distance. Table 1 summarizes the corresponding measuring points. Overall, the total LDV measuring points is 4550 points per configuration (1- LV: $\varphi = 0°$ and 2- LV: $\varphi = 25°$). Taking into consideration the non homogeneous particles seeding, the ITTT (Inter arrival Time and Transit Time) method (Rodriguez et al., 2018) was applied to the LDV data. For more information about this technique, one can refer to Rodriguez et al. (2018).

Table 1. LDV measuring points for the two vehicles.

$d^\star$	$x^\star$	Step $x_s^\star$	Number of points	$y^\star$	Step $y_s^\star$	Number of points
0.93	0.09< $x^\star$ <0.83	0.19	5	0< $y^\star$ <1.02	0.093	12
1.85	0.09< $x^\star$ <1.76	0.19	10			
2.78	0.09< $x^\star$ <1.76	0.19	10			
	1,94< $x^\star$ <2.69	0.37	3			
3.70	0.09< $x^\star$ <1.76	0.19	10			
	2.13< $x^\star$ <2.50	0.37	2			
	3.06< $x^\star$ <3.61	0.56	2			
4.63	0.09< $x^\star$ <1.76	0.28	7	$y^\star$ =1.2	(-)	1
	2.13< $x^\star$ <3.98	0.37	6			
	$x^\star = 4.54$	(-)	1			
5.56	0.09< $x^\star$ <1.76	0.28	7			
	2.13< $x^\star$ <5.46	0.55	7			

3.2. 3C SPIV DATA

The SPIV measurements are undertaken downstream of the square back Ahmed body (LV, $\varphi = 0°$) and the fast back Ahmed body (LV, $\varphi = 25°$) for the six different configurations described above in section 3.1. For each LV($\varphi = 0°$ and $\varphi = 25°$) velocity measurements were acquired between LV and FV in a 2D domain which spreads from $-0.04 < y^* = \frac{y}{h_c} < 1.75$ and $0.04 < x^* <\sim 0.97\ d^*$. Additional LDA measurements are only performed for LV ($\varphi = 0°$) when $d^* = 0.93$ and for LV ($\varphi = 25°$) when $d^* = 0.46$ at the middle distance between the two vehicles.

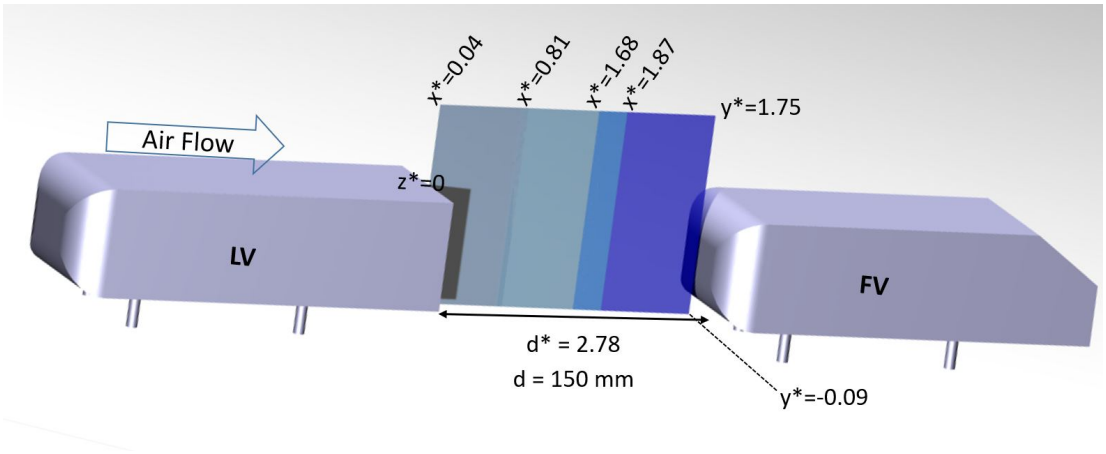

Figure 4. Example of SPIV measurements plans downstream the square Ahmed body.

4. Results

4.1. From LDV data

Figure 5 represents the 2D map of the normalized magnitude of the velocity ($\|\vec{u^*}\| = \sqrt{\bar{u}^{*2} + \bar{v}^{*2}}$, with $u^* = \frac{u}{U_\infty}$ and $v^* = \frac{u}{U_\infty}$) downstream the two cases LV ($\varphi = 0°$ and $\varphi = 25°$) for $z^* = \frac{z}{h_c} = 0$) and for the six inter-vehcile distances.

Firstly, the velocity vectors downstream the square Ahmed body in the Figure 5a indicate two counter-rotating structures in the near wake. The upper structure is clockwise, while the lower one is counter-clockwise. A symetric shape is reflected with respect to $y^* = 0.5$. A large similar low velocity region is observed in the near wake ($x^* = \frac{x}{h_c} <\sim 2$) for $d^* = \frac{d}{h_c} \geq 3.70$. However, for $d^* \leq 2.78$, this region occupies all the inter-vehicle distance. The white dashed lines represent the boundaries of the recirculation region ($u^* = \frac{u}{U_\infty} < 0$). Above $d^* = 2.78$, the length of the recirculation region is almost constant (L_r =1.4 h_c). Comparing with the single vehicle case (Rodriguez, 2018)(for which $L_r^* = \frac{L_r}{h_c}$ = 1.39), the variation of this length does not exceed 5%.

Figure 5b refers to as the results with inclined rear slant angle $\varphi = 25°$. Noting that the meaurements were not possible on the rear slant angle. The velocity vectors did not exhibit a symetric

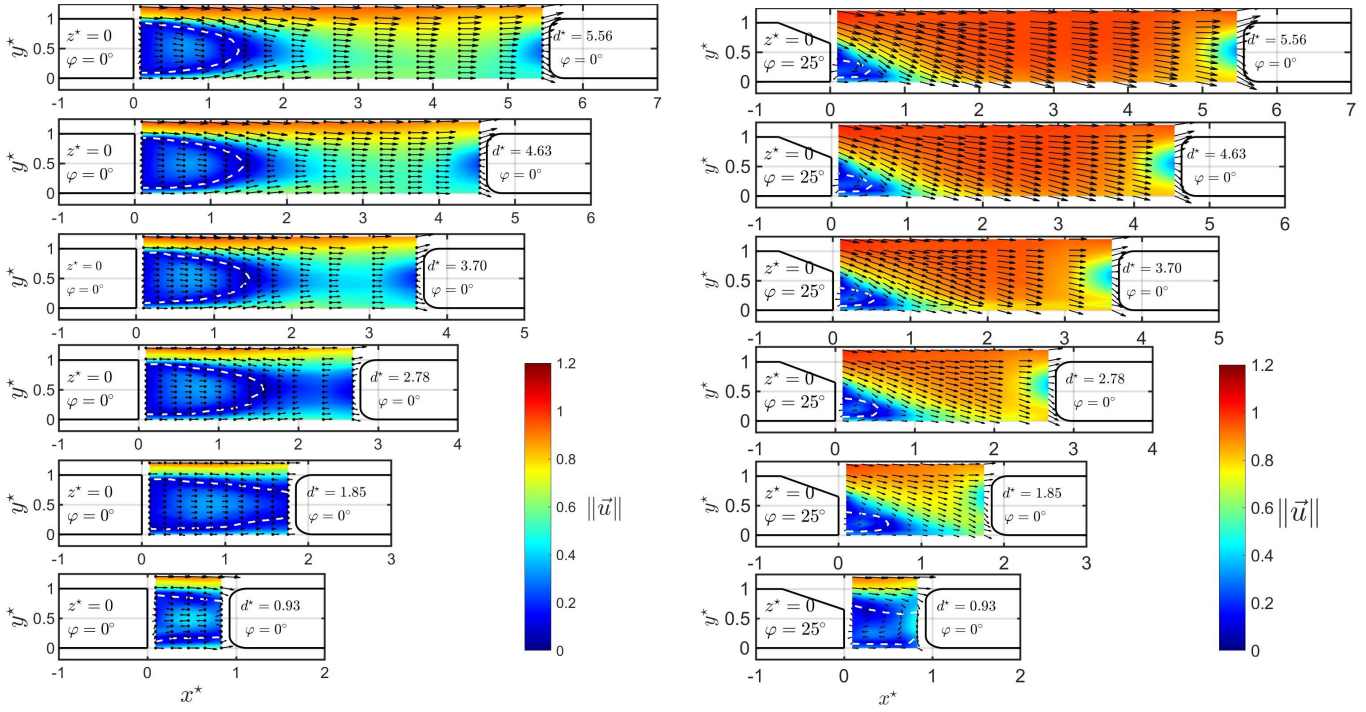

(a) $\varphi = 0°$ (b) $\varphi = 25°$

Figure 5. 2D map of the magnitude of the velocity field for the six configurations.

shape as observed in the wake of square body. A strong downwash effect is observed, which indicates that the flow is fully attached on the rear angle. Regarding the recirculation region, its length is shorter than that measured for the first case LV ($\varphi = 0°$). For $d^* = 1.85$, $L_r = \sim 0.55\ h_c$. Above this distance, it remains almost constant. The deviation of the recirculation region length is less than 6% with respect to the single vehicle case measured in the works of Rodriguez (2018), for which $L_r = 0.58\ h_c$.

Figure 6 summarizes the normalized Turbulent Kinetic Energy fields ($TKE^* = \frac{1}{2}\frac{u'^2 + v'^2}{U_\infty^2}$, such that u' and v' refer to as the fluctuations of horizontal and vertical velocity components, respectively) in the wake of the two Ahmed bodies for the six inter-vehicle distances in the symmetry plane ($z^* = 0$). The black dots represent the meshgrid.

Figure 6a shows the normalized TKE downstream the LV, for which $\varphi = 0°$. The important levels of TKE^* are measured at the boundaries of the recirculation regions (white dashed lines) in the upper shear layer. However, we notice a lower turbulent activity in the lower shear layer, which can be explained by the ground clearance (Rodriguez, 2018). The TKE reaches a peak of $0.065\ U_\infty^2$ for $d^* = 0.93$ at $x^* = 0.46$ and $y^* = 0.93$. From $d^* = 2.78$, the TKE^* fields remain similar.

For LV with $\varphi = 25°$ (Figure 6b), the highest levels of TKE are located in the lower shear layer near to the ground resulting from the strong downash effect. TKE peak values are $0.067U_\infty^2$ and $0.061U_\infty^2$ measured for $d^* = 4.63$ and $d^* = 0.93$, respectively.

From the analysis of the Figures 5 and 6, one can conclude that a critical treshold distance can be defined for each case. Above this distance, the influence of the FV is negligible on the wake prop-

erties between the two vehicles. For LV with $\varphi = 0°$, the critical distance is 2.78 h_c, and for LV with $\varphi = 25°$, it is 1.85 h_c.

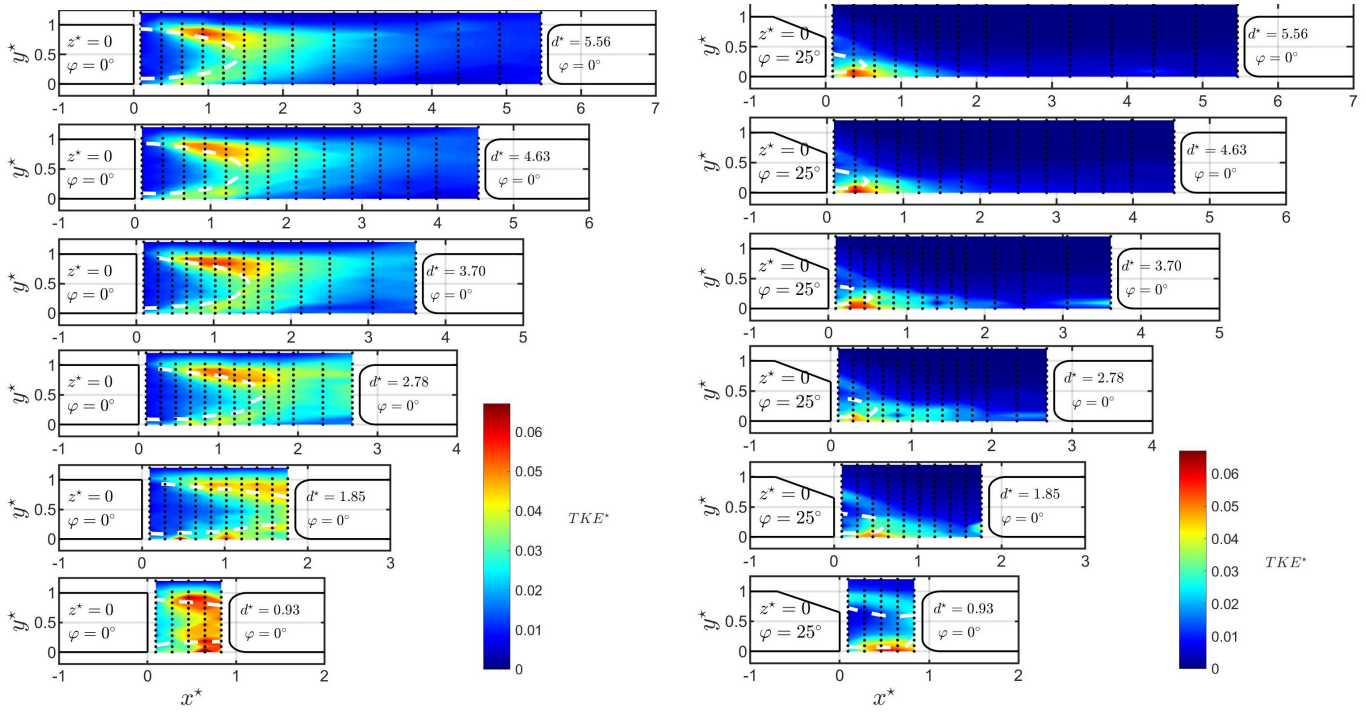

(a) $\varphi = 0°$ (b) $\varphi = 25°$

Figure 6. 2D map of the turbulent kinetic energy for the six configurations.

In order to analyse more in depth the inter-vehicle flow properties, we now present results provided by SPIV technique for LV having $\varphi = 0°$ and for an inter-vehicle distance $d^* = 0.93$, 1.85 and 3.70.

4.2. From SPIV data

4.2.1. Validation with open wind tunnel

Figure 7, Fig. 8 and Fig. 9 show the 2D map of the horizontal velocity in the symmetric plan ($z^* = 0$) downstream the square back car model ($\varphi = 0°$) measured with LDV (a) and SPIV (b) for d^* = 0.93, 1.85 and d^* = 3.70, respectively. It proves that the experimental setup was well-designed and calibrated. Indeed, for d^* = 0.93 and 1.85, the recirculation zone occupies all the available space between the LV and FV (Fig. 7 and Fig. 8). A similar confirmation is observed in Fig. 9a comparing to Fig. 9b. The length of the recirculation region is about 1.47 h_c (Fig. 9a) and 1.3 h_c (Fig. 9b), which corresponds to a difference of about 11%.

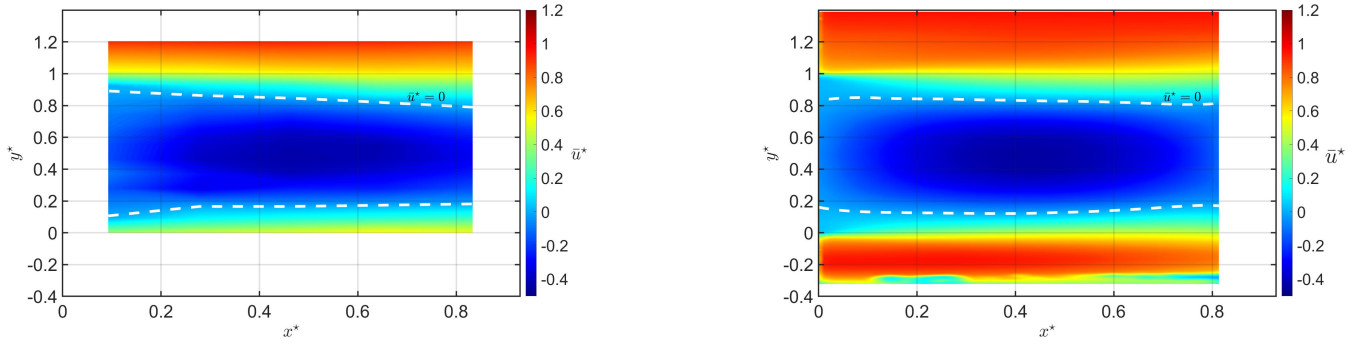

(a) LDV measurements

(b) SPIV measurements

Figure 7. 2D map of the horizontal velocity downstream LV, $\varphi = 0°$ for $d^* = 0.93$.

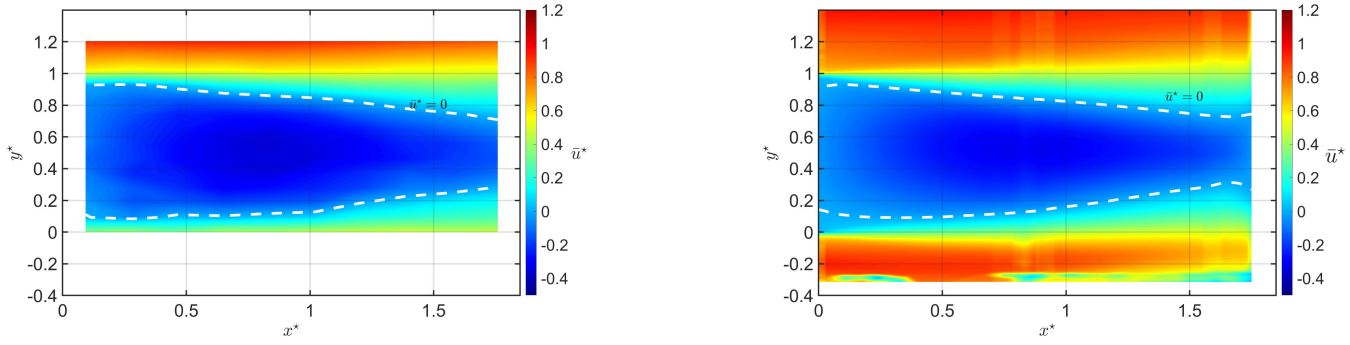

(a) LDV measurements

(b) SPIV measurements

Figure 8. 2D map of the horizontal velocity downstream LV, $\varphi = 0°$ for $d^* = 1.85$.

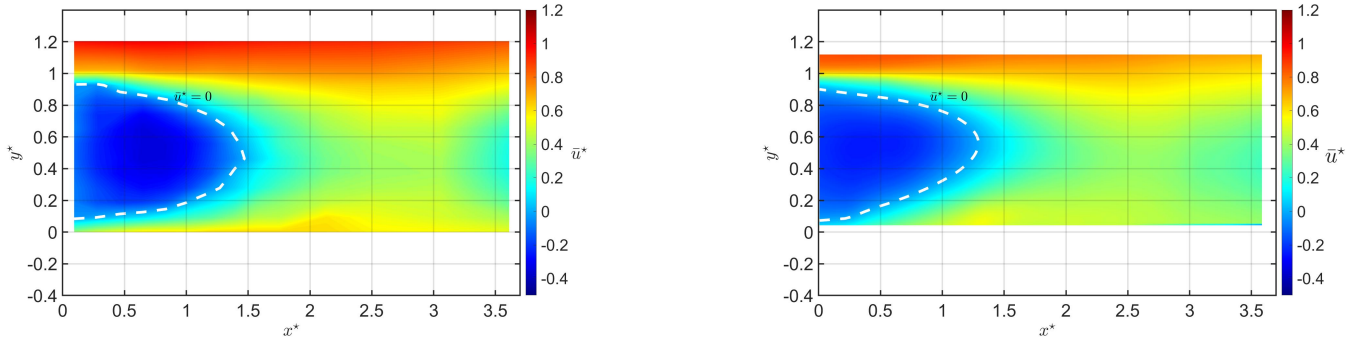

(a) LDV measurements

(b) SPIV measurements

Figure 9. 2D map of the non dimmensional horizontal velocity downstream LV, $\varphi = 0°$ for $d^* = 3.70$.

4.2.2. Bi-stability phenomenon

In addition to the validation of LDV measurements, SPIV data provide complementary information about the transverse component of the velocity vector (w). When placing the following vehicle

dowsntream the square back car model at $d^* = 0.93$ (which is below the length of the recirculation region), we remark that a bi-stability behavior occurs when lookinging at the time seriesof w (Fig. 10a and Fig. 10b). These results diverge from those obtained by Rodriguez (2018), who found that the average transverse velocity was almost negligible downstream the models.

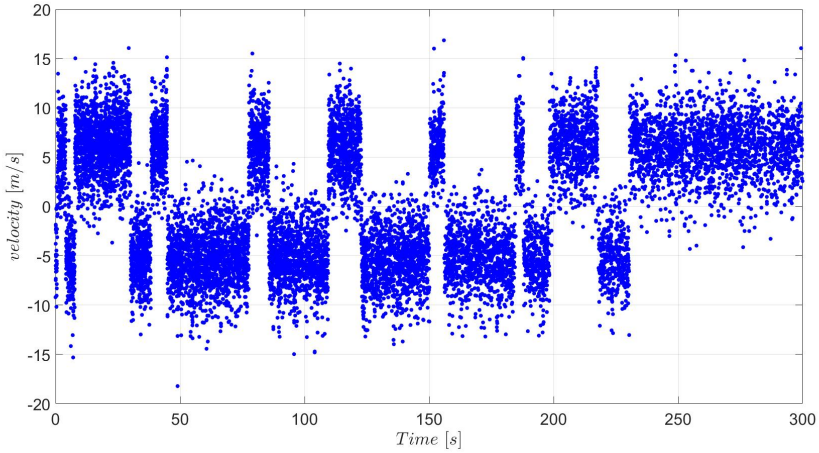

(a) Transverse velocity w

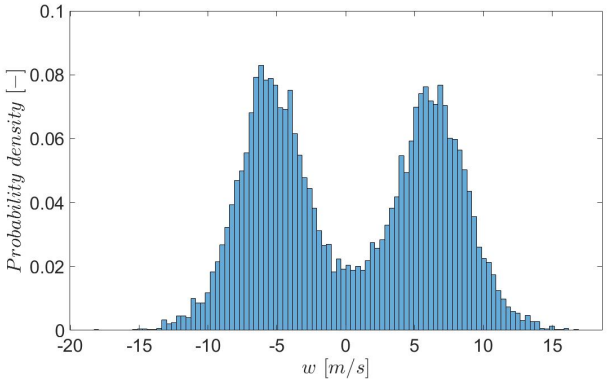

(b) Probability density

Figure 10. Time evolution and associated probability density distribution of the transverse velocity downstream the square model in the midpoint between the vehicles for $d^* = 0.93$.

In order to go further in the analysis of the involved phenomena, LDA measurements in the middle point of the inter-vehicle distance are performed. Figure 10a displays an example of the time series of the raw signal for w. It shows that the values of the tranverse velocity switch from positive $15\,\mathrm{m\,s^{-1}}$ to negative $-15\,\mathrm{m\,s^{-1}}$ values. The shift appears to be a random phenomenon and no proper frequency can be defined. This bi-stable behavior can be seen on the PDF (Probability Distribution Function) associated and in average, the transverse velocity in null (Fig. 10b). It may rely on the presence of the FV in the recirculation region of the wake downstream the LV. It is clearly obvious that the average of w is inappropriate. Having that in mind, SPIV measurements downstream the square back model when the inter-vehicle distance measures 0.93 h_c are correlated with LDA measurements. Three categories of measurements can be distingushed: one when w is

positive (Fig. 11a), second when w is negative (Fig. 11b) and third when it switches from positive to negative states (Fig. 12). We remind that this behavior is seen only seen when LV is a square back model and for $d^* = 0.93$. For d^* = 1.85, the values of the transverse velocity (w) oscillate between $-6\,\mathrm{m\,s^{-1}}$ and $-6\,\mathrm{m\,s^{-1}}$ affording a reliable neglibile average for all cases (See Fig. 13). This trend is valid for all cases when $d^* > 0.93$.

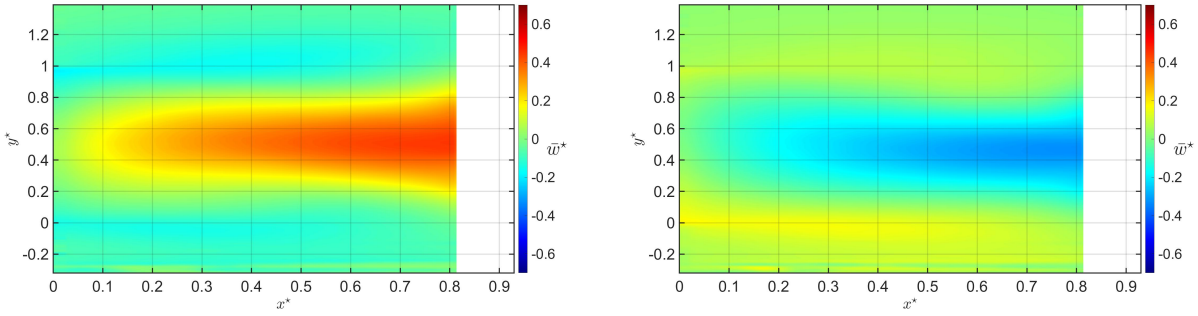

(a) Positive zone

(b) Negative zone

Figure 11. 2D map of the non dimensional transverse mean velocity downstream LV, $\varphi = 0°$ for $d^* = 0.93$.

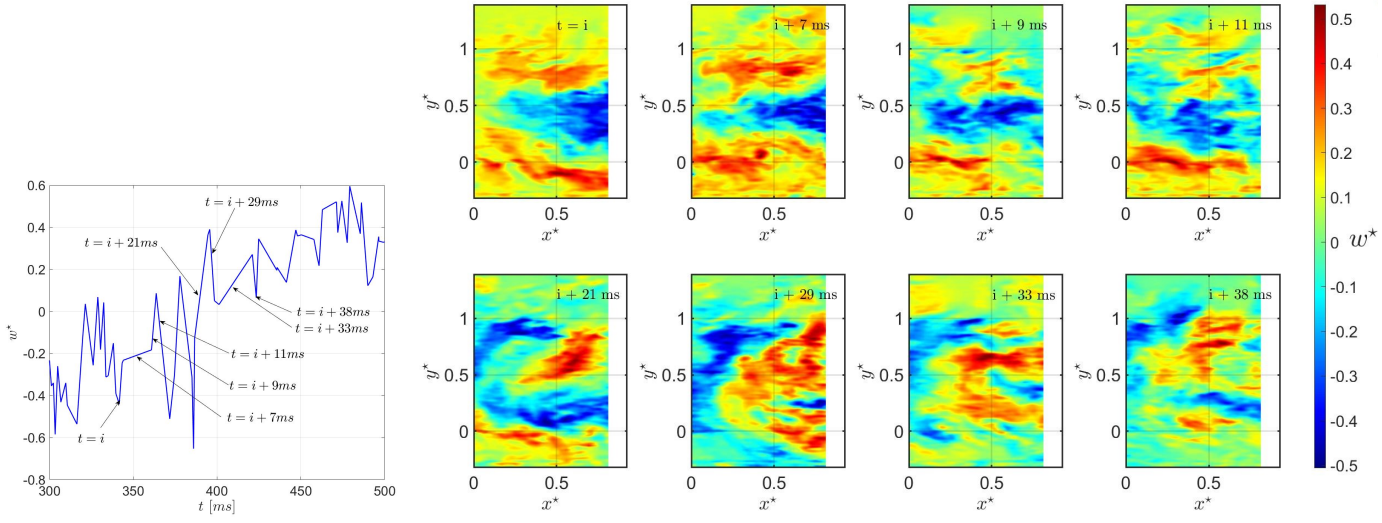

Figure 12. 2D maps of instanteneous transverse velocity in the symmetric plane ($z^* = 0$) downstream the square back car model for d^* = 0.93. The different 2D maps are taken at time i, i+7 ms, i+9 ms, i+11 ms, i+21 ms, i+29 ms, i+33 ms, i+38 ms, respectively.

The instanteneous 2D maps of w^* for the switching from negative to positive values are illustrared in Fig. 12. They are taken from a test for t = i, i+7 ms, i+9 ms, i+11 ms, i+21 ms, i+29 ms, i+33 ms, i+38 ms. From these 2D maps, the fluctuations between the negative values of w^* (first three 2D maps from the first line) and the positive ones (first three 2D maps from the second line) are clearly seen (Fig. 12, left).

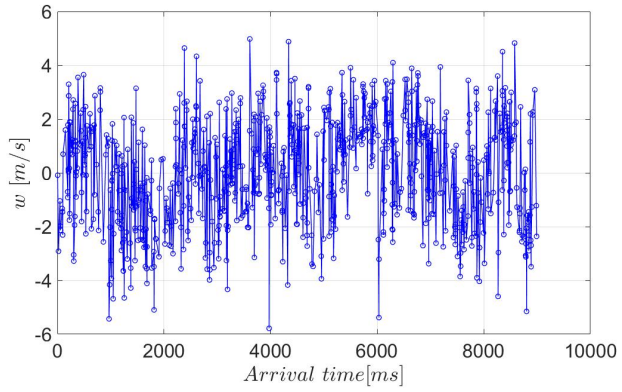

Figure 13. Time evolution of the transverse velocity downstream the square back car model ($\varphi = 0°$) in the midpoint between the vehicles for $d^* = 1.85$

The bi-stability behavior is not figured out when the leading vehicle has a rear slant angle of $\varphi = 25°$ even if the following is located in the recirculation zone ($d^* < 0.58$) (See Fig. 14).

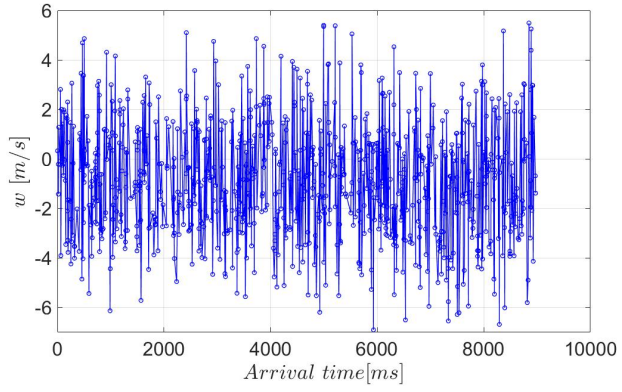

Figure 14. Time evolution of the transverse velocity downstream the fastback car model ($\varphi = 25°$) in the midpoint between the vehicles for $d^* = 0.46$

5. Conclusions

In this paper, an experimental investigation of the flow developping downstream two Ahmed bodies with two different rear slant angles (φ = 0° and 25°) considering the presence of the following vehicle has been carried out by means of LDV and Stereo PIV. The upstream velocity is $14.3\,\mathrm{m\,s^{-1}}$ leading to a Reynolds number of 49500 based on the height of the car model. The influence of the rear slant angle is highlighted. The analysis of the results showed that for d = 2.78 h_c and 1.85 h_c, the influence of the FV is negligible on the mean and turbulent properties measured in the wake of the LV of $\varphi = 0°$ and φ = 25°, respectively. The SPIV results not only validate the LDV measurements, but give also complementary information especially for the transverse component of the velocity vector (w). For LV having a square back ($\varphi = 0°$), a bi-stable behavior is depicted when placing the FV in the recirculation zone ($d^* = 0.93 < 1.40$). In this case, SPIV measurements

are correlated with LDA data. Three cases are described: a first one when w is positive, a second one when w is negative and a third one when w switches from negative to positive. For the other experimental conditions, the transverse velocity is negligible.

Acknowledgements

The financial support of the University of Rouen, the Regional council of Normandy (France) and ESTACA are warmly acknowledged.

Nomenclature

U_∞	Upstream velocity, $14.3\,\mathrm{m\,s^{-1}}$
h_c	Height of the car model [mm]
u	Horizontal component of velocity [m s^{-1}]
v	Vertical component of velocity [m s^{-1}]
w	Transversal component of velocity [m s^{-1}]
d	Inter- vehicle distance [mm]
φ	Rear slant angle of the car model [°]
LV	Leading Vehicle
FV	Following Vehicle
LDV	LASER Doppler Velocimetry (2C)
SPIV	Stereo - Particle Image Velocimetry (3C)
LDA	LASER Doppler Anemometry (1C)
TKE	Turbulent Kinetic Energy
$.*$	Normalized quantities with respect to U_∞ for velocities and with respect to h_c for distances

References

Ahmed, S. R., Ramm, G., & Faltin, G. (1984). Some salient features of the time-averaged ground vehicle wake. *SAE Transactions*, 473–503.

Algieri, A., Bova, S., & De Bartolo, C. (2005). Experimental and numerical investigation on the effects of the seeding properties on lda measurements.

Essel, E., Das, S., & Balachandar, R. (2020). Effects of rear angle on the turbulent wake flow between two in-line ahmed bodies. *Atmosphere*, *11*(4), 328.

Grandemange, M., Gohlke, M., & Cadot, O. (2013). Turbulent wake past a three-dimensional blunt body. part 1. global modes and bi-stability. *Journal of Fluid Mechanics*, *722*, 51–84.

Herry, B. B., Keirsbulck, L., Labraga, L., & Paquet, J.-B. (2011). Flow bistability downstream of three-dimensional double backward facing steps at zero-degree sideslip. *Journal of Fluids Engineering*, *133*(5).

Leclerc, C. (2008). *Réduction de la traînée d'un véhicule automobile simplifié à l'aide du contrôle actif par jet synthétique* (Unpublished doctoral dissertation).

Lienhart, H., & Becker, S. (2003). Flow and turbulence structure in the wake of a simplified car model. *SAE transactions*, 785–796.

Rodriguez, R. (2018). *Etude expérimentale de la dispersion de particules ultrafines dans le sillage de modèles simplifiés de véhicules automobiles* (Unpublished doctoral dissertation). École centrale de Nantes.

Rodriguez, R., Murzyn, F., Aubry, J., Mehel, A., & Larrarte, F. (2018). An innovative ldv data processing method for statistical error corrections. application to homogeneous and non-homogeneous seeding. *Flow Measurement and Instrumentation*, *60*, 67–77.

Rodriguez, R., Murzyn, F., Mehel, A., & Larrarte, F. (2020). Dispersion of ultrafine particles in the wake of car models: A wind tunnel study. *Journal of Wind Engineering and Industrial Aerodynamics*, *198*, 104109.

Spohn, A., & Gilliéron, P. (2002). Flow separations generated by a simplified geometry of an automotive vehicle. , *1*.

Thacker, A., Aubrun, S., Leroy, A., & Devinant, P. (2012). Effects of suppressing the 3d separation on the rear slant on the flow structures around an ahmed body. *Journal of Wind Engineering and Industrial Aerodynamics*, *107*, 237–243.

Torjesen, I. (2021). Fossil fuel air pollution blamed for 1 in 5 deaths worldwide. *BMJ*, *372*. Retrieved from `https://www.bmj.com/content/372/bmj.n406` doi:

West, G., & Apelt, C. (1982). The effects of tunnel blockage and aspect ratio on the mean flow past a circular cylinder with reynolds numbers between 104 and 105. *Journal of Fluid mechanics*, *114*, 361–377.